



Published in final edited form as:

Biochemistry. 2011 March 29; 50(12): 2092–2100. doi:10.1021/bi200109q.

Cholesterol 5,6-secosterol Aldehyde Adduction to Membrane-Bound Myelin Basic Protein Exposes an Immunodominant Epitope[†]

Natalie K. Cygan[‡], Johanna C. Scheinost[‡], Terry D. Butters[§], and Paul Wentworth Jr.^{*,‡,||,⊥}

[‡]The Scripps-Oxford Laboratory, University of Oxford, South Parks Road, Oxford OX1 3QU, UK

[§]The Oxford Glycobiology Institute, Department of Biochemistry, University of Oxford, South Parks Road, Oxford OX1 3QU, UK

^{||}Department of Chemistry, The Scripps Research Institute, 10550 N. Torrey Pines Road, La Jolla, CA, U.S.A.

[⊥]The Skaggs Institute for Chemical Biology, The Scripps Research Institute, 10550 N. Torrey Pines Road, La Jolla, CA, U.S.A.

Abstract

Myelin degradation in the CNS is a clinical hallmark of multiple sclerosis (MS). A reduction in the net positive charge of myelin basic protein (MBP) *via* deimination of arginine to citrulline, has been shown to correlate strongly with disease severity and has been linked to myelin instability and a defect that precedes neurodegeneration and leads to autoimmune attack. Recently, we have shown that lipid-derived aldehydes, such as the cholesterol 5,6-secosterols atheronal-A (**1a**) and atheronal-B (**1b**), modulate the misfolding of certain proteins such as apolipoprotein-B₁₀₀, β-amyloid, α-synuclein, and κ- and λ-antibody light chains in a process involving adduction of the hydrophobic aldehyde to lysine side-chains, resulting in a loss in net positive charge of the protein. In this study we show that the presence of either atheronal-A (**1a**) or atheronal-B (**1b**) in large unilamellar vesicles (cyt-LUVs) comprised of the lipid composition found in the cytosolic myelin sheath and bovine MBP (bMBP), leads to an atheronal concentration dependent increase in the surface exposure of the immunodominant epitope (V86-T98) as determined by antibody binding. Other structural changes in bMBP were also observed, specifically **1a–b** induces a decrease in the surface exposure of L36-P50 relative to control cyt-LUVs as measured both by antibody binding and by a reduction in cathepsin D proteolysis of F42-F43. Structure activity relationship studies with analogs of **1a** and **1b** point to the aldehyde moiety of both compounds being critical to their effects on bMBP structure. The atheronals also cause a reduction in the size of the bMBP-cyt-LUV aggregates, as determined by fluorescence microscopy and dynamic light scattering. These results suggest that imine formation between inflammatory-derived aldehydes, that effectively reduces the cationic nature of MBP, can lead to structural changes in MBP and a decrease in

[†]This work was supported by the NIH (AG28300), The Scripps Research Institute (PW) and The Skaggs Institute for Chemical Biology (PW).

*To whom correspondence should be addressed. Telephone: +1-858-784-2576. Fax: +1-858-784-7385. paulw@scripps.edu; paul.wentworth@bioch.ox.ac.uk.

SUPPORTING INFORMATION

Supporting material available is the DLS data for cyt-LUVs containing the oxysterol analogs **2a–3b**. This material is available free of charge via the Internet at <http://pubs.acs.org>.

myelin stability akin to deimination and as such may be a hitherto unknown contributory aspect to the onset and progression of MS.

Multiple sclerosis (MS) is an inflammatory demyelinating autoimmune disease characterized by degradation of the central nervous system (CNS) myelin sheath, resulting in chronic and progressive neurological impairment (1). The classical MS lesions contain T and B lymphocytes and macrophages that are reactive against myelin antigens. The protein responsible for adhesion and stabilization of the intracellular surfaces of compact multilayered myelin, is myelin basic protein (MBP) ($pI \sim 10$) which accounts for approximately 30% of the total myelin protein (2–5) (Figure 1A). Structurally, MBP is an 18.5 kDa intrinsically unstructured protein, with its structural orientation being highly dependent upon its environment (6–8). Only subtle changes in the amount or ratio of lipid composition in membranes results in myelin disruption as a result of changes in the electrostatic forces between the negatively charged cytoplasmic membrane surfaces and positively charged MBP (9).

MBP shows extensive post-translational modification (PTM) with degrees of deimination, phosphorylation, deamidation, methylation and *N*-terminal acylation. These modifications give rise to charge variant isoforms C1–C8, of which C1 is the least modified and most cationic isomer and is the most abundant form of MBP in healthy adult humans. Critically, the least cationic component is C8, with extensive deimination of arginine residues, is elevated in patients with MS, relative to age matched healthy controls (10,11). Deimination (the conversion of positively charged arginine to uncharged citrulline) (Figure 1B) diminishes the ability of MBP to cause adhesion of lipid bilayers through electrostatic interactions and has a direct correlation to disease severity (2,3,5,7,10–20). Using a recombinant murine MBP isoform with R or K (at a locus in the murine sequence that corresponds to R in the human protein) → Q mutations to mimic the citrullination of human MBP, Harauz and co-workers (21) showed that the immunodominant epitope (V83–T92, murine sequence numbering) was more solvent exposed in the maximally deiminated isoform (*rmC8*) relative to the least deiminated isoform (*rmC1*). This peptide sequence represents the minimal epitope for T cell recognition of human MBP (V86–T98, human sequence numbering) with the highest affinity for MHC class II haplotype, HLA-DR, believed to be associated with increased risk of MS (22). Thus the current thinking in the field is that a reduction in the cationic status of hMBP induces changes in the structure and function of this critical protein that renders it unable to perform its role of compaction and maintenance of the integrity of the myelin sheath and makes it a target for autoimmune attack (23).

Recently, we have discovered a new class of cholesterol oxidation products termed the atheronals **1a–b** *in vivo* (24,25) (Figure 2). Aldehydes **1a–b** are chemically unique as oxysterols, because the steroid nucleus is disrupted at C5–C6. Both atheronal-A and atheronal-B have been isolated from atherosclerotic plaque material (24), the systemic levels of **1b** are elevated in patients with advanced atherosclerosis and critically from the perspective of MS, the CNS levels of **1b** are elevated in patients with an inflammatory neurological disease, Lewy Body dementia (26). Thus, both the local and systemic levels of the atheronals are related to the combination of cholesterol levels and inflammatory status (24) (27,28). What makes the atheronals of potential importance in the context of this study is that they have been shown to modulate the misfolding of a number of disease-related proteins such as apolipoprotein-B₁₀₀ (24), β -amyloid (29–31), α -synuclein (26), antibody light chains (32), and a murine prion protein (33) *via* a process that involves, in part, adduction to specific lysine side-chains in the sequence to form imines (Schiff bases) (Figure 1C) (30). This process essentially reduces the cationic charge of the protein and

elevates the local hydrophobicity of these adducted proteins. These effects combine to either trigger or inhibit misfolding events in susceptible proteins.

Herein, we show that the presence of atheronal-A and atheronal-B in cyt-LUVs leads to an increase in the surface exposure of the immunodominant epitope (V83-T95, bovine sequence numbering) and a decrease in surface exposure of the cathepsin-D binding domain (L36-P50, bovine sequence numbering) relative to control cyt-LUVs. In addition the atheronals reduce the size and structural stability of bMBP-induced aggregates. Both these atheronal-induced effects are analogous to those observed with deimination and hint at a potential role for lipid-aldehyde mediated adduction to MBP in the onset and severity of MS.

MATERIALS AND METHODS

Reagents

Bovine myelin basic protein (bMBP) was isolated and purified from bovine brain white matter as previously described (34). The bMBP used for these studies was > 95 % pure as measured by analytical HPLC. Phosphatidylcholine (PC), phosphatidylethanolamine (PE), phosphatidylinositol (PI), and sphingomyelin (sphing) were used as supplied by Sigma-Aldrich. Cholesterol (chol) and phosphatidylserine (PS) were supplied by Matraya and were used without further purification. Atheronal-A (3 β -hydroxy-5-oxo-5,6-secocholestan-6-al) (**1a**), atheronal-B (3 β -hydroxy-5 β -hydroxy-B-norcholestane-6 β -carboxaldehyde) (**1b**), ketoacid **2a** and ketoalcohol **3a** were synthesized as previously described (24).

Synthesis of 3 β -hydroxy-5 β -hydroxy-B-norcholestane-6 β -carboxylic acid (**2b**)

Acid **2b** was synthesized by adapting a protocol by Smith and Leenay (35). In brief, aldehyde **1b** (42 mg, 0.1 mmol) was dissolved in tetrahydrofuran (THF) (2.5 ml) containing 2-methyl-2-butene (350 mg, 5 mmol; 2 M solution in THF). The mixture was then treated dropwise with an aqueous solution (1 ml) of 80 % sodium chlorite (91 mg, 1 mmol) and monobasic sodium phosphate (84 mg, 0.7 mmol). The reaction mixture was stirred vigorously for 2 h at room temperature, and then the organic solvent was removed *in vacuo*. The aqueous residue was extracted with ethyl acetate (4 \times 10 ml), the combined organic layers were dried with sodium sulphate and the solvent evaporated to dryness. The resulting crystals were washed with hexanes to give **2b** as a white solid (38 mg, 87 %). ¹H NMR (500 MHz, CDCl₃) δ 4.05 (m, 1H, H-3), 2.23 (d, 1H, *J* = 10.0 Hz, H-6), 0.94 (s, 3H, CH₃-19), 0.89 (d, 3H, *J* = 7.0 Hz, CH₃-21), 0.843 (d, 3H, *J* = 7.0 Hz, CH₃), 0.839 (d, 3H, *J* = 7.0 Hz, CH₃), 0.68 (s, 3H, CH₃-18); ¹³C NMR (125.72 MHz, CDCl₃) δ 178.02, 82.95, 67.42, 58.74, 56.66, 55.92, 51.50, 45.56, 44.86, 44.84, 42.85, 39.89, 39.71, 36.44, 35.85, 28.63, 28.44, 28.23, 24.31, 24.07, 23.01, 22.76, 21.72, 18.99, 17.78, 12.73. HR-ESI-MS (ESI+): found 435.3477 [M+H]⁺, found 457.3288 [M+Na]⁺; calculated for C₂₇H₄₇O₄: 435.3474, calculated for C₂₇H₄₆O₄Na: 457.3294.

Synthesis of 3 β -hydroxy-5 β -hydroxy-B-norcholestane-6 β -hydroxymethyl (**3b**)

Sodium borohydride (38 mg, 1 mmol) was added to a solution of **1b** (42 mg, 0.1 mmol) in methanol (1 ml), and allowed to stir at room temperature for 3 h. The crude material was purified as is by preparative TLC [ethyl acetate – hexane (2:3)] and the desired product eluted from the silica using ethyl acetate. Evaporation of the solvent yielded **3b** as a clear oil (19 mg, 45 %). ¹H NMR (500 MHz, CDCl₃) δ 4.12 (m, 1H, H-3), 3.77 (s, 1H, CH₂-OH), 3.66 (dd, 1H, *J* = 10.0 Hz, 10.0 Hz, H_a-7), 3.56 (dd, 1H, *J* = 10.0 Hz, 4.0 Hz, H_b-7), 3.27 (s, 1H, 3 β -OH), 2.34 (s, 1H, 5 β -OH), 0.92 (s, 3H, CH₃-19), 0.91 (d, 3H, *J* = 7.0 Hz, CH₃-21), 0.864 (d, 3H, *J* = 7.0 Hz, CH₃), 0.860 (d, 3H, *J* = 7.0 Hz, CH₃), 0.65 (s, 3H, CH₃-18); ¹³C NMR (125.27, CDCl₃) δ 84.06, 67.98, 65.10, 56.87, 55.84, 54.72, 50.18, 45.40, 45.23,

44.90, 40.38, 40.16, 39.74, 36.48, 35.86), 28.85, 28.33, 28.24, 26.94, 24.74, 24.06, 23.02, 22.78, 21.66, 19.08, 19.02, 12.76. HR-ESI-MS (ESI⁺): found 443.3496 [M+Na]⁺; calculated for C₂₇H₄₈O₃Na: 443.3501.

Preparation of large unilamellar vesicles (LUVs)

LUVs were prepared as previously described (13,36). Briefly, aliquots of lipid solutions in chloroform were combined in the desired molar ratio and evaporated *in vacuo*. LUVs were composed of a lipid mixture similar to that of the cytoplasmic monolayer of myelin (Cyt : LUVs) consisting of chol : PE : PS : PC : sphing : PI at a molar percentage of 44 : 27 : 13 : 11 : 3 : 2 and prepared by probe sonication followed by syringe extrusion (Avanti Polar Lipids) through a polycarbonate membrane (100 nm) 14 times (13,36). Cyt-LUVs were prepared in HEPES (20 mM, pH 7.4) containing NaCl (10 mM) for fluorescence microscopy, dynamic light scattering, and flow cytometry experiments, and sodium acetate (50 mM, pH 4.0) containing NaCl (10 mM) for proteolysis with cathepsin D. It should be noted for studies with cyt-LUVs containing oxysterols **1a–3b**, the molar % of oxysterol replaced an equimolar amount of cholesterol.

Flow Cytometry (FCM)

Two *loci* on the bMBP protein were probed by FCM, the immunodominant epitope (V86-T92, bovine sequence numbering) and the primary cathepsin-D binding domain (L36-P50, bovine sequence numbering). Thus, bMBP was added to 1 mL of cyt-LUVs (HEPES, 20 mM, NaCl, 10 mM, pH 7.4) (1 mg/mL) containing **1a–b**, **2a–b** or **3a–b** (0, 10, 20, or 30 μM, equivalent to 0, 0.25, 0.5 or 0.75 mol % respectively) at a protein:lipid ratio of 1 : 600. The solution was incubated at room temperature for 30 min to ensure complete aggregation. A murine monoclonal antibody (Abcam, ab22460), which binds specifically to the bMBP immunodominant epitope (V86-T92) or a rat monoclonal antibody (Millipore, MAB395) which binds to L36-P50 of bMBP, was then added at a 1/100 dilution and incubated at room temperature for 30 min, followed by incubation with a fluorophore-tagged secondary antibody (Invitrogen, A21202 or A11006) for an additional 30 min at a 1/1000 dilution. Once the primary and secondary antibodies were added to the solution, FACS analysis was performed using a FACScan flow cytometer (Becton and Dickinson) with the threshold set to 900, and the MFI calculated from three collections of 10,000 counts. Three separate runs were completed to allow statistical analysis to be performed.

Digestion of lipid-associated bMBP with cathepsin D

Bovine cathepsin D (100 ng, Calbiochem) was added to a suspension of cyt-LUVs (10 μL, 6 mg/mL) containing bMBP at a molar protein : lipid ratio of 1 : 600 and into which had been incorporated **1a–b**, **2a–b**, or **3a–b** (0, 10, 20 or 30 μM equivalent to 0, 0.25, 0.5 or 0.75 mol % respectively) in sodium acetate buffer (50 mM, pH 4.0) (21). Each sample was inverted twice and flushed with argon (1 min). Aliquots were taken during the incubation at given times (0 to 24 h). The enzymatic reaction was stopped by adding NuPage LDS loading buffer (4X, 4 μL, Invitrogen) followed by incubation at 110 °C (5 min). The mixture was then resolved by Bis-Tris PAGE (10%) (Invitrogen) and visualized by Coomassie staining. Densitometry was performed for quantitative comparison using a Fuji LAS1000Pro Intelligent Dark Box II CCD camera (Düsseldorf, Germany) and analyses was carried out using Advanced Image Data Analyser (AIDA) software (Straubenhardt, Germany).

Fluorescence microscopy of ThT-treated bMBP-Cyt-LUV aggregates

bMBP was added to cyt-LUVs containing varying amounts of **1a** or **1b** (0, 10, 20, or 30 μM equivalent to 0, 0.25, 0.5 or 0.75 mol % respectively) at a molar protein : lipid ratio of 1 : 600 in aqueous buffer [HEPES (20 mM), NaCl (10 mM); pH 7.4] (50 μL, 6 mg/mL).

Thioflavin T (ThT) (50 μ M) was added to the solution and incubated at room temperature for 30 min after which the solution was transferred to a slide and sealed with a cover slip. The slides were analyzed on a Zeiss Axioplan epifluorescence microscope (Carl Zeiss, Brighton, UK) and images were captured using a cooled CCD camera (Carl Zeiss, Brighton, UK) and metamorph software. Three representative images for each sample were taken.

Dynamic light scattering of bMBP-Cyt-LUV aggregates

bMBP-Cyt-LUV aggregate size distribution was determined using a Viscotek 802 dynamic light scattering (DLS) instrument (Houston TX). bMBP was added to cyt-LUVs (1 mL, 2.5 μ M) into which was incorporated **1a** or **1b** (30 μ M, 0.75 mol %) of at a 1 : 600 protein : lipid ratio and incubated at room temperature for 30 min and then transferred to a quartz cuvette. Scattered light was detected at a 90° angle and data was obtained from 10 measurements of 5 s duration and averaged utilizing the instrumental software to determine aggregate distribution. The average size for each type of aggregate was determined using data collected from three separate runs.

RESULTS

Inclusion of atheronals (**1a–b**) into cyt-LUVs increases the surface exposure of the immunodominant epitope (V86-T98) of bMBP

Flow cytometry (FCM) was used as a minimally disruptive approach for assessing protein domain exposure on the surface of bMBP cyt-LUV aggregates in the presence or absence of **1a–b**. Thus, in order to assess whether **1a** or **1b** incorporated in cyt-LUVs affects the surface exposure of the immunodominant epitope (V86-T98) at a protein:lipid ratio found within myelin, an FCM experiment was designed. This FCM approach was considered superior to the more standard ELISA-based experiment for this study because FCM is able to measure antibody binding at regions of bMBP without compromising the integrity of the aggregates by the necessity of mounting them onto a surface such as a microtiter plate. In addition, the threshold of the FACS instrument can be set to measure only large aggregates, ensuring that the measured fluorescence only originates from the primary antibody bound to the immunodominant epitope of fused cyt-LUVs. Prior to in-depth FCM studies, a preliminary analysis was performed which confirmed there were no measurable differences in fluorescence intensity associated with the different cyt-LUV compositions when the oxysterols **1a–3b** are incorporated. Having thus validated the FCM method for this study, individual histograms of aggregate count versus fluorescence intensity were then measured for complexation of an anti-immunodominant epitope monoclonal antibody to bMBP-loaded cyt-LUVs comprising of increasing amounts (0–0.75 mol %) of each of **1a–3b** (Figure 3A). This analysis revealed a concentration-dependent increase in anti-epitope (V86-T98) antibody binding, as measured by fluorescence emission, upon inclusion of the cholesterol 5,6-*secosterols* **1a–b** into the cyt-LUVs (Figure 3B). Thus, inclusion of 0.75 mol % of **1a** or **1b** leads to an ~ 3 fold increase in the measured mean fluorescence intensity relative to control cyt-LUVs (**1a** = 1023 \pm 48; **1b** = 934 \pm 42; control = 407 \pm 42). In contrast, there is no significant increase in the mean fluorescence emission relative to control cyt-LUVs containing MBP when any of the oxysterol atheronal analogs, **2a**, **2b**, **3a** and **3b** are incorporated into LUVs up to the maximum concentration studied, 0.75 mol % (Figure 3B).

Incorporation of atheronals (**1a–b**) into cyt-LUVs decreases cathepsin-D primary site (F42-F43) proteolysis of bMBP

In our hands, bMBP (~18.5 kDa) in cyt-LUVs is almost entirely cleaved by cathepsin D at the primary proteolysis site (F42-F43) after 24 h incubation in sodium acetate (50 mM, pH 4.0) at 37°C. This site-specific proteolysis releases a 14.5 kDa protein fragment, and can be followed routinely by SDS-PAGE (Figure 4). Inclusion of atheronals **1a** and **1b** into the

bMBP-containing cyt-LUVs, leads to a concentration-dependent reduction in the time-dependant cathepsin-D-mediated cleavage of bMBP as determined by quantification of the 14.5 kDa band density (Figure 4). Thus, with the incorporation of **1a** or **1b** (10 μ M, 0.25 mol%) into the cyt-LUVs there is a decrease in digestion to 65.4 and 80.1 % respectively of that observed with control cyt-LUVs (Figure 4C). With **1a** or **1b** at 20 μ M (0.5 mol %) in the cyt-LUVs, this reduction falls to 55.8 and 59.4 % of control cyt-LUVs. At the highest concentration of **1a** and **1b** studied (30 μ M, 0.75 mol %), the proteolysis is 42.1 and 43.2 % of control cyt-LUV cleavage respectively. In contrast, incorporation of the atheronal analog compounds **2a–3b** up to 30 μ M into ct-LUVs has no measurable effect on cathepsin-D proteolysis of bMBP.

Incorporation of atheronals (1a–b) into cyt-LUVs decreases surface exposure of L36-P50 containing the cathepsin-D primary cleavage site (F42-F43) of bMBP

The primary cathepsin-D cleavage site (F42-F43) is present within the L36-P50 domain for which there is a commercially available rat mAb (MAB395). Thus, the FCM method developed above was modified to measure oxysterol-mediated effects on solvent exposure of the L36-P50 sequence of bMBP (Figure 4D). Inclusion of aldehydes **1a–b** into cyt-LUVs containing MPB resulted in a concentration-dependent reduction in MFI associated with L36-P50 binding of the mAb (MAB395). In contrast, when the oxysterol analogs **2a–3b** are incorporated into cyt-LUVs, there is no effect on surface exposure of L36-P50 as measured by FCM.

bMBP-cyt-LUV aggregates that contain 1a–b have altered morphology

In general, MBP induces aggregation of cyt-LUVs almost instantaneously to form multilayer aggregates similar to those found in the myelin sheath (5,37,38). Incorporation of the fluorescent dye thioflavin-T and fluorescence microscopy was used to determine the morphological characteristics of these MBP-Cyt-LUV aggregates in the presence and absence of aldehydes **1a–b** (Figure 5). Long fibrous aggregates (> 1mm in length) are typically formed when MBP is added to cyt-LUVs, and are similar in appearance to those found in the myelin sheath (Figure 5a and e). However, upon addition of increasing concentrations of **1a** or **1b** into the cyt-LUVs, the morphology of the aggregates changes dramatically, becoming less fibrous, smaller and more spherical in appearance (Figure 5b–d and Figure 5f–h).

bMBP-Cyt-LUV aggregate size distribution is reduced in the presence of oxysterols 1a and 1b

Dynamic light scattering (DLS) was employed to gain quantitative data on the size of bMBP-Cyt-LUV aggregates in the presence and absence of **1a** or **1b**. MBP-induces aggregates of cyt-LUVs of one major size (997 ± 28 nm), comprising of ~ 96% of the total aggregates observed (Table 1). The addition of 30 μ M of **1a** or **1b** within the cyt-LUVs resulted in a dramatic reduction in aggregate size to either 431 ± 90 nm or 464 ± 54 nm respectively. There was also an increase in the percentage of even smaller aggregates in the oxysterol incorporated cyt-LUVs; 69 ± 43 nm (25% of aggregates, **1a**) and 126 ± 38 nm (~42 % of aggregates, **1b**).

DISCUSSION

In search of a potential role for oxysterol aldehyde adduction to CNS proteins and autoimmune pathogenesis, we have extended our studies of cholesterol 5,6-*secosterols* **1a** and **1b** mediated protein misfolding (29–31,33,39), to MBP. As detailed above, it is now clearly established that a reduced cationic nature of MBP, through PTMs such as deimination (R \rightarrow Q) (Figure 1), and phosphorylation *via* mitogen-activated protein kinase

(MAPK) (40) correlate strongly with MS disease severity (10,11). At the structural level, it has been shown that this neutralization in charge of MBP causes significant changes in protein conformation, exposing immunodominant B and T-cell epitopes (21,23), renders the protein susceptible to proteolysis (12,15,41), reduces its ability to both cause adhesion of apposed membranes, and to tether the Fyn-SH3 domain to membranes (42), and even leads to membrane fragmentation (15–17).

Our group and others have shown that adduction of oxysterols **1a–b** with the primary amine side chain of K residues in peptides and proteins (29,30,32,33), or phosphatidylethanolamine in membrane phospholipids (43,44) involves Schiff-base formation, which is a formal neutralization of cationic charge (Figure 1c). Therefore the question became, does adduction of aldehydes **1a–b** to native MBP in myelin-like membranes *in vitro* induce similar structural changes in MBP that have been linked to the pathological effects ascribed to PTMs *in vivo*? The work we report here suggests that the answer to this question is yes. Thus, we have shown that upon replacement of cholesterol with increasing amounts of oxysterols **1a** and **1b** (0.25–0.75 mol %) in bMBP-aggregated Cyt-large unilamellar vesicles (LUVs), used to mimic the cytoplasmic leaflet of the myelin membrane, there is an oxysterol concentration-dependent increase in the liposome membrane surface exposure of the minimal epitope for T cell recognition of MBP (V86-T98; V85-T97 bovine numbering) (Figure 3). This segment of the protein has the highest affinity for the MHC class II haplotype, HLA-DR, believed to be associated with increased susceptibility to MS (22,45,46). The T and B cells found in the CNS of MS patients show specificity for this minimal epitope, and antibodies against it are found in both the brain and spinal fluid of MS patients, emphasizing the humoral and cellular responses to this epitope in disease pathogenesis (46,47).

A concern when designing this study was being able to assess any potential non-specific effects on MBP that may result from substitution of cholesterol in the cyt-LUVs for the more hydrophilic oxysterols **1a** and **1b**. It should be pointed out that substitution of cholesterol was enforced for two reasons, primarily to mimic the *in vivo* case where we envision cholesterol being oxidized by ROS to form **1a** and **1b**. The second, to maintain a precise MBP/lipid ratio of 1:600 known to ensure complete association between MBP and cyt-LUVs (21). To help answer this concern of changing the biophysical characteristics of the LUVs, a panel of close structural analogues to oxysterols **1a–b** were also studied for their effects on MBP orientation in liposomal membranes. From a chemical point of view there are a number of important features included in the analogues. First, ring B of the oxysterols is either open (**2a** and **3a**), to allow mimicry of atheronal-A (**1a**), or fused (β -hydroxy acid **2b** and γ -hydroxyalcohol **3b**) for simile with atheronal-B (**1b**). Second, the aldehyde group, essential for Schiff base formation, is replaced with either an isopolar (dipole \rightarrow dipole) non isosteric ($sp^2 \rightarrow sp^3$ carbon hybridization) hydroxyl group (**3a** and **3b**) or an isosteric ($sp^2 \rightarrow sp^2$ carbon hybridization) non-isopolar (dipole \rightarrow anion at pH > 5) carboxyl group (**2a** and **2b**) (Figure 2). The essential point was to replace the locus for Schiff base formation with a moiety of either similar charge or shape. Importantly, there was no measurable effect on surface exposure of the immunodominant epitope of MBP when these analogues were incorporated in the cyt-LUVs in the concentration range effective for **1a** and **1b** (0.25–0.75 mol %). This lack of effect of the analogues **2a–3b** allows us to conclude with a high degree of certainty that the effect of **1a–1b** on MBP conformation in the liposomal membrane must at least in part be due to aldehyde-mediated adduction to K residues in the protein sequence. Another fair conclusion from the study with analogues is that non-aldehyde containing oxysterols are generally ineffective at mediating changes in MBP orientation within membranes. This is an important observation because, with the exception of **1a** and **1b**, this covers all currently known biologically-relevant oxysterols (48). Generally oxysterols are hydroxylated at various *loci* around the sterol nucleus or on the alkyl side-chain. There are

higher oxidation products known, such as 7-ketocholesterol but even this one is largely unreactive with proteins.

Another clear effect of the atheronals **1a** and **1b** on MBP conformation in cyt-LUVs is a concentration dependent reduction in solvent exposure of the primary cathepsin D (EC 3.4.23.5) proteolysis site (F42-F43 bovine numbering) (Figure 4). Cathepsin D cleaves MBP primarily between F42-F43 site and secondarily between F86-F87 in the immunodominant epitope (49,50). Single cleavage at the F42-F43 releases a β -peptide ($M_r \sim 14.4$ kDa), in a process that can be followed by quantifying band density on SDS-PAGE. This reduction in F42-F43 cleavage of MBP in **1a** and **1b**-containing LUVs was corroborated by a reduction in binding of an anti-L36-P50 rat monoclonal antibody, measured by FCM. These two pieces of data combined point to the fact that this region, L36-P50 is buried to a greater extent in the cyt-LUVs containing **1a** and **1b** than normal cyt-LUVs. Incorporation of the oxysterol analogs **2a-3b** had no effect on either F42-F43 cleavage by cathepsin D, or exposure of the L36-P50 domain. A recent study by Harauz and co-workers has shown that a highly citrullinated form of MBP, termed *rmC8*, is cleaved ~ 3 fold faster in the F42-F43 site than a native uncitrullinated MBP (21). Here then is a clear contrast, between the effect of citrullination and lipid aldehyde adduction, but one that is not too surprising. MBP is an intrinsically unfolded protein, whose orientation and folding to secondary structural elements are highly dependent upon local environment. Thus, multiple R \rightarrow Q PTMs causes increased surface exposure of L36-P50, making the protein susceptible to proteolysis by cathepsin D in a process linked to release of the immunodominant epitope V86-T98; (V85-T97 bovine numbering) after secondary proteolysis. Whereas, atheronal-adduction to lysine side chains of MBP buries the L36-P50 site, while simultaneously exposing the immunodominant epitope V86-V98 on the surface of the membrane.

Aggregation of cyt-LUVs by bMBP *in vitro* occurs by charge-charge non-covalent association between one LUV and another. This interaction is due to association between the highly positively charged protein (MBP +19) and the negatively charged phospholipid head groups on the solvent exposed surfaces of the cyt-LUVs. Consequently, long fibrous aggregates (~ 1 μ m in length) are typically formed and we have measured these aggregates by both fluorescence microscopy (Figure 5) and dynamic light scattering (DLS) (Table 1). Incorporation of **1a** or **1b** into the cyt-LUVs causes a dramatic reduction in the size and causes a change in shape of the MBP-induced Cyt-LUV aggregates from linear fiber-like to spheres (Figure 5). Clearly, given the importance of charge-charge interactions for stabilizing apposing membranes, atheronal-adduction and neutralization of lysine side chain cationic charge may well weaken membrane-membrane interactions and hence not allow for large aggregates to form. In addition, an EPR spectroscopy study has shown that the immunodominant epitope region of the protein is highly amphipathic comprising of hydrophobic amino acids on one side and polar amino acids on the other side of an α -helix (51,52). This segment is generally buried in the lipid bilayer due to a hydrophobic-hydrophilic residue ratio of 13 : 5 and plays an important role in anchoring the protein in the membrane (53). Therefore, given that the atheronals cause such a dramatic change in surface exposure of the immunodominant epitope *vide supra*, this could well weaken the ability of MBP to anchor itself to the lipid membranes and hence the cause the morphological changes observed. Furthermore, the structure-activity relationship compounds **2a-3b** when incorporated into cyt-LUVs cause similar morphological changes, showing that the integrity of the myelin is disrupted by the presence of oxysterol compounds not specifically **1a-b**.

Having shown that atheronals **1a-b** in cyt-LUVs can cause such dramatic changes in MBP conformation and function in membranes; exposing the immunodominant epitope V86-T98, burying the L36-P50 domain and reducing aggregate size *in vitro* it is important now to consider how this process, lipid aldehyde induced MBP misfolding, may be relevant *in vivo*.

We have shown that the atheronals are present in all CNS samples, brain and CSF, and are elevated in Lewy body disease, another inflammatory neurological disorder (26). It is clear that inflammation plays a major role in the pathogenesis of multiple sclerosis (54). Abundant lipid content and high oxygen consumption make the brain particularly susceptible to free radical-mediated peroxidation and hence lipid aldehyde formation, such as the atheronals (55,56). In addition, cholesterol is a major lipid component of the myelin, constituting ~ 27.7% of total lipid (56,57). This high level of cholesterol coupled with inflammation and elevated reactive oxygen species (ROS) in MS patients provides an optimal environment for the generation of **1a–b**. And so, while the actual levels of **1a** and **1b** are not yet known in MS patients, it is certain these reactive aldehydes will be there.

In summary, we have shown that the biologically-relevant cholesterol 5,6-secosterol aldehydes, atheronal-A **1a** and atheronal-B **1b** cause structural changes in MBP when incorporated into cyt-LUVs that leads to exposure of an immunodominant epitope and causes a reduction in aggregate size and changes in morphology reminiscent of the changes observed in MS. While the *in vivo* relevance of this process is still to be unraveled, it is clear that this process of lipid aldehyde adduction to MBP may well be a hitherto unheralded mechanism of autoimmune pathogenesis in MS.

Supplementary Material

Refer to Web version on PubMed Central for supplementary material.

Abbreviations

bMBP	bovine myelin basic protein
hMBP	human myelin basic protein
PC	phosphatidylcholine
PE	phosphatidylethanolamine
PS	phosphatidylserine
PI	phosphatidylinositol
sphingo	sphingomyelin
cyt-LUVs	large unilamellar vesicles mimicking the cytoplasmic monolayer of myelin
ThT	thioflavin T
DLS	dynamic light scattering
CNS	central nervous system
THF	tetrahydrofuran

Acknowledgments

The authors would like to thank all members of the Wentworth group (TSRI and SOL) for assistance and suggestions during this work and Mutchmeats Ltd, UK for providing the bovine brain samples for MBP purification.

REFERENCES

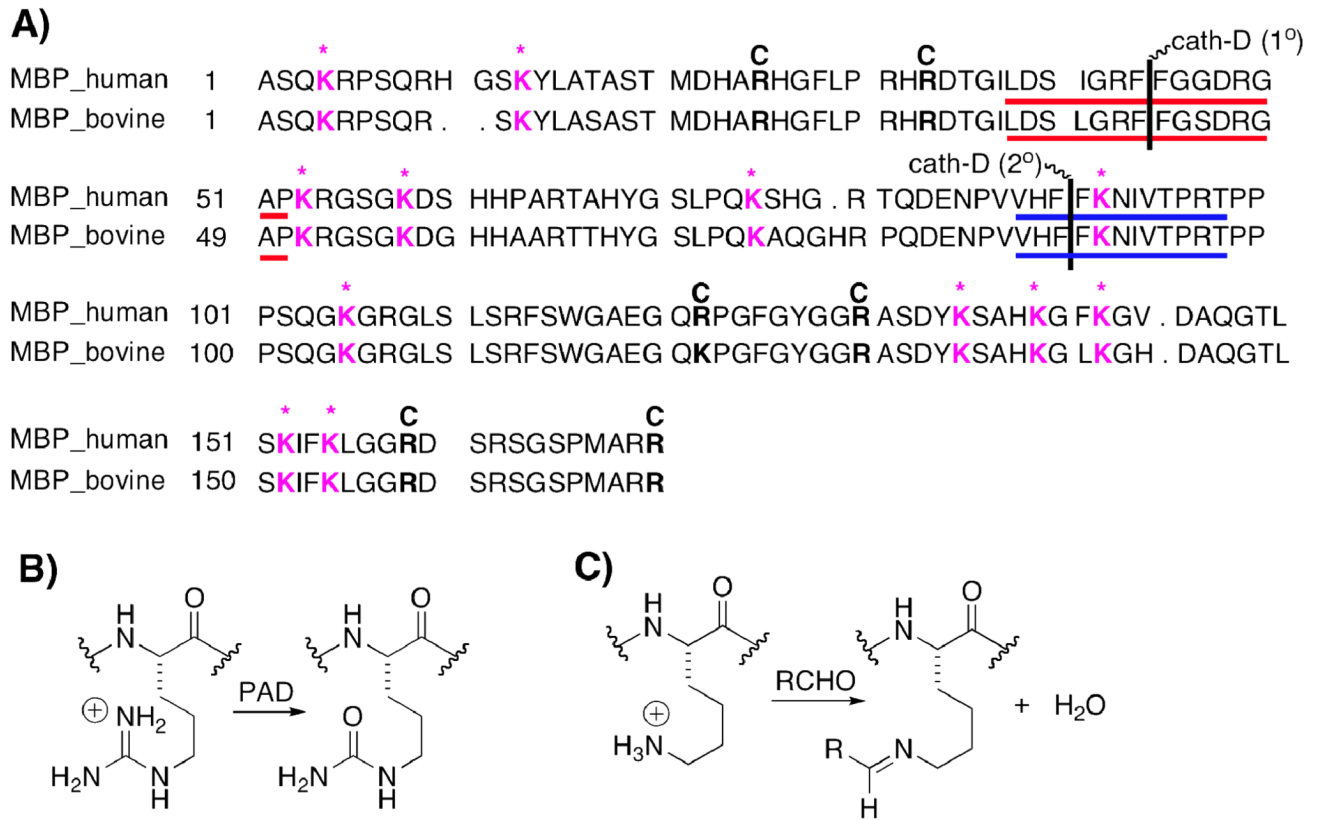
1. Boggs JM. Myelin basic protein: a multifunctional protein. *Cellul. Mol. Life Sci.* 2006; 63:1945–1961.

2. Readhead C, Takasashi N, Shine HD, Saavedra R, Sidman R, Hood L. Role of myelin basic protein in the formation of central nervous system myelin. *Ann. N. Y. Acad. Sci.* 1990; 605:280–285. [PubMed: 1702601]
3. Omlin FX, Webster HD, Palkovits CG, Cohen SR. Immunocytochemical localization of basic protein in major dense line regions of central and peripheral myelin. *J. Cell Biol.* 1982; 95:242–248. [PubMed: 6183269]
4. Harauz G, Ishiyama N, Hill CMD, Bates IR, Libich DS, Fares C. Myelin basic protein--diverse conformational states of an intrinsically unstructured protein and its roles in myelin assembly and multiple sclerosis. *Micron.* 2004; 35:503–542. [PubMed: 15219899]
5. Brady GW, Murthy NS, Fein DB, Wood DD, Moscarello MA. The effect of basic myelin protein on multilayer membrane formation. *Biophys. J.* 1981; 34:345–350. [PubMed: 6165412]
6. Tompa P. Intrinsically unstructured proteins. *TiBS.* 2002; 27:527–533. [PubMed: 12368089]
7. Bates IR, Matharu P, Ishiyama N, Rochon D, Wood DD, Polverini E, Moscarello MA, Viner NJ, Harauz G. Characterization of a recombinant murine 18.5-kDa myelin basic protein. *Protein Expres. Purif.* 2000; 20:285–299.
8. Polverini E, Fasano A, Zito F, Riccio P, Cavatorta P. Conformation of bovine myelin basic protein purified with bound lipids. *Eur. Biophys. J.* 1999; 28:351–355. [PubMed: 10394626]
9. Hu Y, Doudevski I, Wood D, Moscarello M, Husted C, Genain C, Zasadzinski JA, Israelachvili J. Synergistic interactions of lipids and myelin basic protein. *Proc. Natl. Acad. Sci. U. S. A.* 2004; 101:13466–13471. [PubMed: 15353595]
10. Moscarello MA, Wood DD, Ackerley C, Boulias C. Myelin in multiple sclerosis is developmentally immature. *J. Clin. Invest.* 1994; 94:146–154. [PubMed: 7518827]
11. Wood DD, Bilbao JM, O'Connors P, Moscarello MA. Acute multiple sclerosis (Marburg type) is associated with developmentally immature myelin basic protein. *Ann. Neurol.* 1996; 40:18–24. [PubMed: 8687186]
12. Bates IR, Libich DS, Wood DD, Moscarello MA, Harauz G. An Arg/Lys-->Gln mutant of recombinant murine myelin basic protein as a mimic of the deiminated form implicated in multiple sclerosis. *Protein Expres. Purif.* 2002; 25:330–341.
13. Boggs JM, Yip PM, Rangaraj G, Jo E. Effect of posttranslational modifications to myelin basic protein on its ability to aggregate acidic lipid vesicles. *Biochemistry.* 1997; 36:5065–5071. [PubMed: 9125528]
14. Wood DD, Moscarello MA. The isolation, characterization, and lipid-aggregating properties of a citrulline containing myelin basic protein. *J. Biol. Chem.* 1989; 264:5121–5127. [PubMed: 2466844]
15. Beniac DR, Wood DD, Palaniyar N, Ottensmeyer FP, Moscarello MA, Harauz G. Cryoelectron microscopy of protein-lipid complexes of human myelin basic protein charge isomers differing in degree of citrullination. *J. Struct. Biol.* 2000; 129:80–95. [PubMed: 10675299]
16. Boggs JM, Rangaraj G, Koshy KM. Analysis of the membrane-interacting domains of myelin basic protein by hydrophobic photolabeling. *Biochimica et Biophysica Acta.* 1999; 1417:254–266. [PubMed: 10082801]
17. Shanshiashvili LV, Suknidze NC, Machaidze GG, Mikeladze DG, Ramsden JJ. Adhesion and clustering of charge isomers of myelin basic protein at model myelin membranes. *Arch. Biochem. Biophys.* 2003; 419:170–177. [PubMed: 14592460]
18. Cheifetz S, Boggs JM, Moscarello MA. Increase in vesicle permeability mediated by myelin basic protein: effect of phosphorylation of basic protein. *Biochemistry.* 1985; 24:5170–5175. [PubMed: 2416340]
19. Cheifetz S, Moscarello MA. Effect of bovine basic protein charge microheterogeneity on protein-induced aggregation of unilamellar vesicles containing a mixture of acidic and neutral phospholipids. *Biochemistry.* 1985; 24:1909–1914. [PubMed: 2410021]
20. MacMillan SV, Ishiyama N, White GF, Palaniyar N, Hallett FR, Harauz G. Myelin basic protein component C1 in increasing concentrations can elicit fusion, aggregation, and fragmentation of myelin-like membranes. *Eur. J. Cell Biol.* 2000; 79:327–335. [PubMed: 10887963]

21. Musse AA, Boggs JM, Harauz G. Deimination of membrane-bound myelin basic protein in multiple sclerosis exposes an immunodominant epitope. *Proc. Natl. Acad. Sci. U. S. A.* 2006; 103:4422–4427. [PubMed: 16537438]
22. Ota K, Matsui M, Milford EL, Mackin GA, Weiner HL, Hafler DA. T-cell recognition of an immunodominant myelin basic protein epitope in multiple sclerosis. *Nature.* 1990; 346:183–187. [PubMed: 1694970]
23. Musse AA, Harauz G. Molecular 'negativity' may underline multiple sclerosis: role of the myelin basic protein family in the pathogenesis of MS. *Int. Rev. Neurol.* 2007; 79:149–172.
24. Wentworth P Jr, Nieva J, Takeuchi C, Galve R, Wentworth AD, Dilley RB, DeLaria GA, Saven A, Babior BM, Janda KD, Eschenmoser A, Lerner RA. Evidence for ozone formation in human atherosclerotic arteries. *Science.* 2003; 302:1053–1056. [PubMed: 14605372]
25. Wentworth P Jr, McDunn JE, Wentworth AD, Takeuchi C, Nieva J, Jones T, Bautista C, Ruedi JM, Gutierrez A, Janda KD, Babior BM, Eschenmoser A, Lerner RA. Evidence for antibody-catalyzed ozone formation in bacterial killing and inflammation. *Science.* 2002; 298:2195–2199. [PubMed: 12434011]
26. Bosco DA, Fowler DM, Zhang Q, Nieva J, Powers ET, Wentworth P, Lerner RA, Kelly JW. Elevated levels of oxidized cholesterol metabolites in Lewy body disease brains accelerate [alpha]-synuclein fibrillization. *Nature Chem. Biol.* 2006; 2:249–253. [PubMed: 16565714]
27. Wentworth P Jr, Jones LH, Wentworth AD, Zhu X, Larsen NA, Wilson IA, Xu X, Goddard WA III, Janda KD, Eschenmoser A, Lerner RA. Antibody catalysis of the oxidation of water. *Science.* 2001; 293:1806–1811. [PubMed: 11546867]
28. Wentworth AD, Jones LH, Wentworth P Jr, Janda KD, Lerner RA. Antibodies have the intrinsic capacity to destroy antigens. *Proc. Natl. Acad. Sci. U. S. A.* 2000; 97:10930–10935. [PubMed: 11005865]
29. Zhang Q, Powers ET, Nieva J, Huff ME, Dendle MA, Bieschke J, Glabe CG, Eschenmoser A, Wentworth P Jr, Lerner RA, Kelly JW. Metabolite-initiated protein misfolding may trigger Alzheimer's disease. *Proc. Natl. Acad. Sci. U. S. A.* 2004; 101:4752–4757. [PubMed: 15034169]
30. Scheinost JC, Wang H, Boldt G, Offer J, Wentworth P Jr. Cholesterol *seco*-sterol-induced aggregation of methylated amyloid-beta peptides--insights into aldehyde-initiated fibrillization of amyloid-beta. *Angew Chemie, Int. Ed.* 2008; 47:3919–3922.
31. Bieschke J, Zhang Q, Powers ET, Lerner RA, Kelly JW. Oxidative metabolites accelerate Alzheimer's amyloidogenesis by a two-step mechanism, eliminating the requirement for nucleation. *Biochemistry.* 2005; 44:4977–4983. [PubMed: 15794636]
32. Nieva J, Shafton A, Altabell LJ 3rd, Tripuraneni S, Rogel JK, Wentworth AD, Lerner RA, Wentworth P Jr. Lipid-derived aldehydes accelerate light chain amyloid and amorphous aggregation. *Biochemistry.* 2008; 47:7695–7705. [PubMed: 18578541]
33. Scheinost JC, Witter DP, Boldt GE, Offer J, Wentworth PJ. Cholesterol *seco*sterol adduction inhibits the misfolding of a mutant prion protein fragment that induces neurodegeneration. *Angew Chemie, Int. Ed.* 2009; 48:9469–9472.
34. Miller D, Karpus WJ. Experimental autoimmune encephalomyelitis in the mouse. *Curr. Prot. Immunol.* 2007; 15.11.11–15.11.18.
35. Smith III AB, Leenay TL. Indole diterpene synthetic studies. 5. Development of a unified synthetic strategy; a stereocontrolled, second-generation synthesis of (–)-paspaline. *J. Am. Chem. Soc.* 1989; 111:5761–5768.
36. Inouye H, Kirschner DA. Membrane interactions in nerve myelin: II. Determination of surface charge from biochemical data. *Biophys. J.* 1988; 53:247–260. [PubMed: 3345333]
37. Lampe PD, Wei GJ, Nelsestuen GL. Stopped-flow studies of myelin basic protein association with phospholipid vesicles and subsequent vesicle aggregation. *Biochemistry.* 1983; 22:1594–1599. [PubMed: 6189513]
38. Smith RR. The basic protein of CNS myelin: Its structure and ligand binding. *J. Neurochem.* 1992; 59:1589–1608. [PubMed: 1383423]
39. Bieschke J, Zhang Q, Bosco DA, Lerner RA, Powers ET, Wentworth P Jr, Kelly JW. Small molecule oxidation products trigger disease-associated protein misfolding. *Acc. Chem. Res.* 2006; 39:611–619. [PubMed: 16981677]

40. Erickson AK, Payne DM, Martino PA, Rossomando AJ, Shabanowitz J, Weber MJ, Hunt DF, Sturgill TW. Identification by mass spectrometry of threonine 97 in bovine myelin basic protein as a specific phosphorylation site for mitogen-activated protein kinase. *J. Biol. Chem.* 1990; 265:19728–19735. [PubMed: 1700979]
41. Bates IR, Boggs JM, Feix JB, Harauz G. Membrane anchoring and charge effects in the interaction of myelin basic protein with lipid bilayers studied by site-directed spin labeling. *J. Biol. Chem.* 2003; 278:29041–29047. [PubMed: 12748174]
42. Homchaudhuri L, Polverini E, Gao W, Harauz G, Boggs JM. Influence of membrane surface charge and post-translational modifications to myeline basic protein on its ability to tether the Fyn-SH3 domain to a membrane in vitro. *Biochemistry.* 2009; 48:2385–2393. [PubMed: 19178193]
43. Bach D, Wachtel E, Miller IR. Kinetics of Schiff base formation between the cholesterol ozonolysis product 3 β -hydroxy-5-oxo-5,6-secocholestan-6-al and phsophatidylethanolamine. *Chem. Phys. Lipids.* 2009; 157:51–55. [PubMed: 18948091]
44. Wachtel E, Bach D, Epanand RF, Tishbee A, Epanand RM. A product of ozonolysis of cholesterol alters the biophysical properties of phosphatidylethanolamine membranes. *Biochemistry.* 2006; 45:1345–1351. [PubMed: 16430232]
45. Valli A, Sette A, Kappos L, Oseroff C, Sidney J, Miescher G, Hochberger M, Albert ED, Adorini L. Binding of myelin basic protein peptides to human histocompatibility leukocyte antigen class II molecules and their recognition by T cells from multiple sclerosis patients. *J. Clin. Invest.* 1993; 91:616–628. [PubMed: 7679413]
46. Wucherpennig KW, Sette A, Southwood S, Oseroff C, Matsui M, Strominger JL, Hafler DA. Structural requirements for binding of an immunodominant myelin basic protein peptide to DR2 isotypes and for its recognition by human T cell clones. *J. Exp. Med.* 1994; 179:279–290. [PubMed: 7505801]
47. Martino G, Olsson T, Fredrikson S, Hojeberg B, Kostulas V, Grimaldi LM, Link H. Cells producing antibodies specific for myelin basic protein region 70–89 are predominant in cerebrospinal fluid from patients with multiple sclerosis. *Eur. J. Immunol.* 1991; 21:2971–2976. [PubMed: 1721023]
48. Bjorkem I, Diczfalusy U. Oxsterols: friends, foes or just fellow passengers? *Arterio. Thromb. Vasc. Biol.* 2002; 22:734–742.
49. Cao L, Goodin R, Wood D, Moscarello MA, Whitaker JN. Rapid release and unusual stability of immunodominant peptide 45–89 from citrullinated myelin basic protein. *Biochemistry.* 1999; 38:5374–5381.
50. Pritzker LB, Joshi S, Gowan JJ, Harauz G, Moscarello MA. Deimination of myelin basic protein. 1. Effect of deimination of arginyl residues of myelin basic protein on its structure and susceptibility to digestion by cathepsin D. *Biochemistry.* 2000; 39:5374–5381. [PubMed: 10820008]
51. Mendz GL, Brown LR, Martenson RE. Interactions of myelin basic protein with mixed dodecylphosphocholine/ palmitoyllysophosphatidic acid micelles. *Biochemistry.* 1990; 29:2304–2311. [PubMed: 1692480]
52. Warren KG, Catz I, Steinman L. Fine specificity of the antibody response to myelin basic protein in the central nervous system in multiple sclerosis: the minimal B-Cell epitope and a model of its features. *Proc. Natl. Acad. Sci. U. S. A.* 1995; 92:11061–11065. [PubMed: 7479937]
53. Kitamura A, Kiyota T, Tomohiro M, Umeda A, Lee S, Inoue T, Sugihara G. Morphological behavior of acidic and neutral liposomes induced by basic amphiphilic α -helical peptides with systematically varied hydrophobic-hydrophilic balance. *Biophys. J.* 1999; 76:1457–1468. [PubMed: 10049327]
54. Martino G, Adorini L, Rieckmann P, Hillert J, Kallmann B, Comi G, Filippi M. Inflammation in multiple sclerosis: the good, the bad, and the complex. *Lancet Neurol.* 2002; 1:499–509. [PubMed: 12849335]
55. Bongarzone ER, Soto EF, Pasquini JM. Oxidative damage to proteins and lipids of CNS myelin produced by in vitro generated reactive oxygen species. *J. Neurosci. Res.* 1995; 65:1342–1347.
56. Smith KJ, Kapoor R, Felts PA. Demyelination: the role of reactive oxygen and nitrogen species. *Brain Pathol.* 1999; 9:69–92. [PubMed: 9989453]

57. Saher G, Brugger B, Lappe-Siefke C, Mobius W, Tozawa R-I, Wehr MC, Wieland F, Ishibashi S, Nave K-A. High cholesterol level is essential for myelin membrane growth. *Nature Neurosci.* 2005; 8:468–475. [PubMed: 15793579]

**FIGURE 1.**

A) Aligned amino acid sequences of the 18.5 kDa isoforms of human MBP (hMBP, 170 residues) and bovine MBP (bMBP, 168 residues). The number at the beginning of each row refers to the first residue for that sequence. Gaps are marked by the “.” symbol. In hMBP: R25, R33, R122, R130, R159 and R170 are the sites most often deiminated, giving rise to the C8 isoform which is the predominant form in MS, and are marked with “C” for citrulline. The lysines throughout hMBP and bMBP that may be valid targets for atheronal adduction are marked in pink and with a “*” symbol. The blue underlined segment is the major immunodominant epitope of MBP (V86-T98 human sequence numbering; V85-T97 bovine sequence numbering). The red underlined segment is the MBP cathepsin D (cath-D) binding domain. The primary (1⁰, F44-F45 human sequence numbering; F42-F43 bovine sequence numbering) and secondary (2⁰, F89-F90 human sequence numbering; F88-F89 bovine sequence numbering) cleavage sites of MBP by cathepsin-D are marked with a black solid line between the residues where proteolysis occurs. B) Scheme for enzymatic deimination of an arginine residue to citrulline in a peptide. PAD – peptidyl arginine deiminase. C) Schiff base (imine) formation between a lysine residue and an aldehyde RCHO.

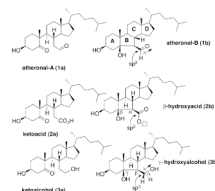


FIGURE 2.

Oxysterols used in this study: atheronal-A (**1a**) and atheronal-B (**1b**) contain a reactive aldehyde moiety which comprises an sp^2 carbon with a dipole. The ketoacid (**2a**) and ketoalcohol (**3a**), β -hydroxyacid (**2b**), γ -hydroxyalcohol (**3b**) are all included as either isosteric ($sp^2 \rightarrow sp^2$), non-isopolar (dipole \rightarrow anion) or non-isosteric ($sp^2 \rightarrow sp^3$) isopolar (dipole \rightarrow dipole) analogs of **1a** and **1b**.

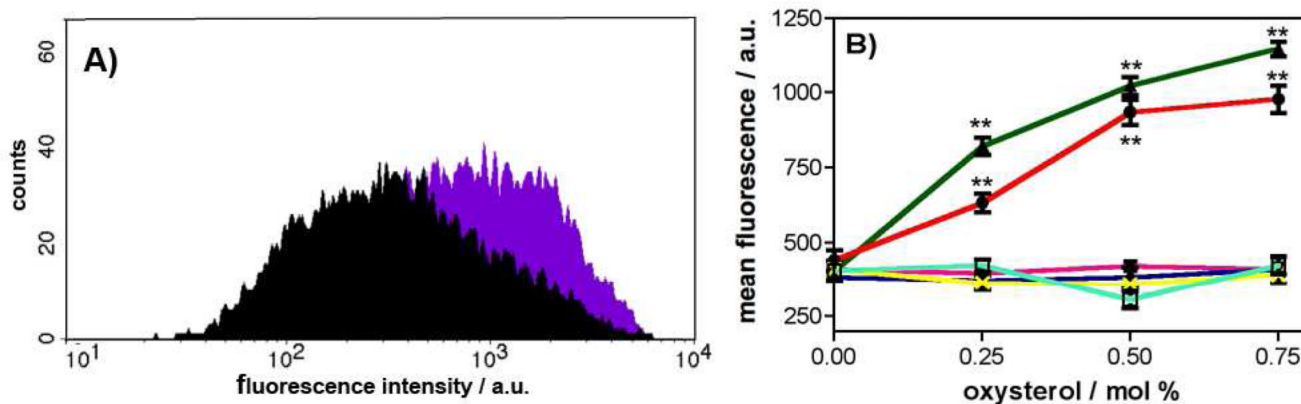
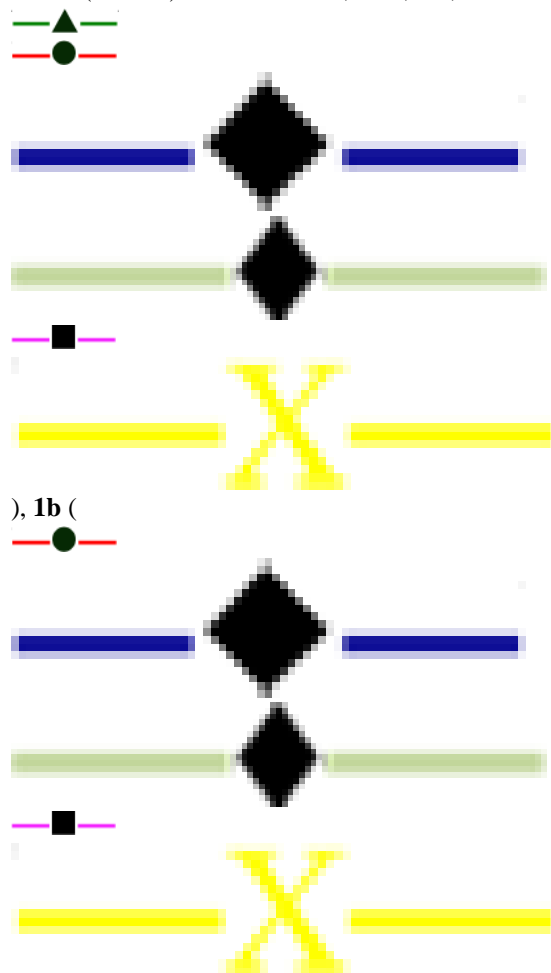
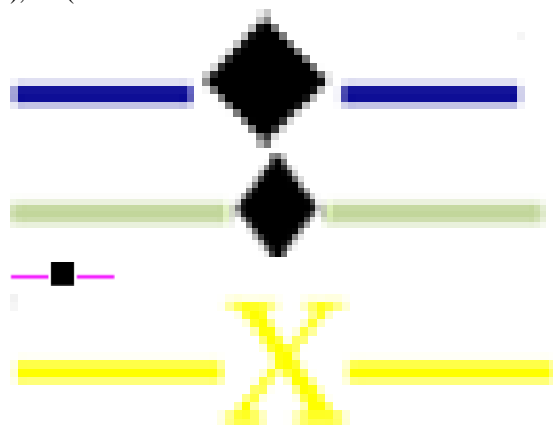
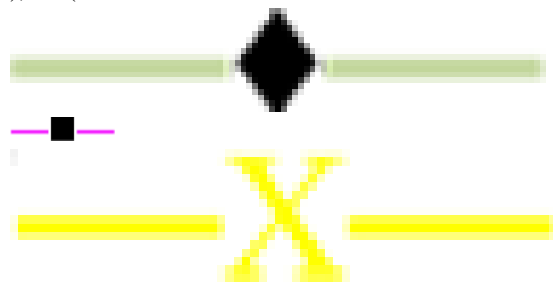
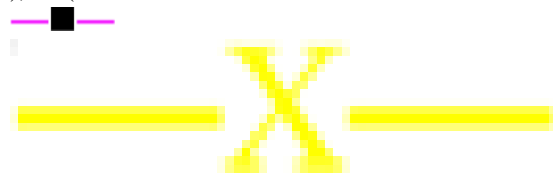
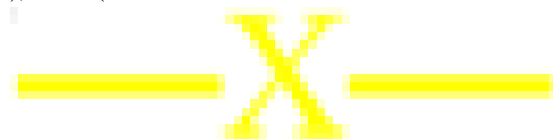


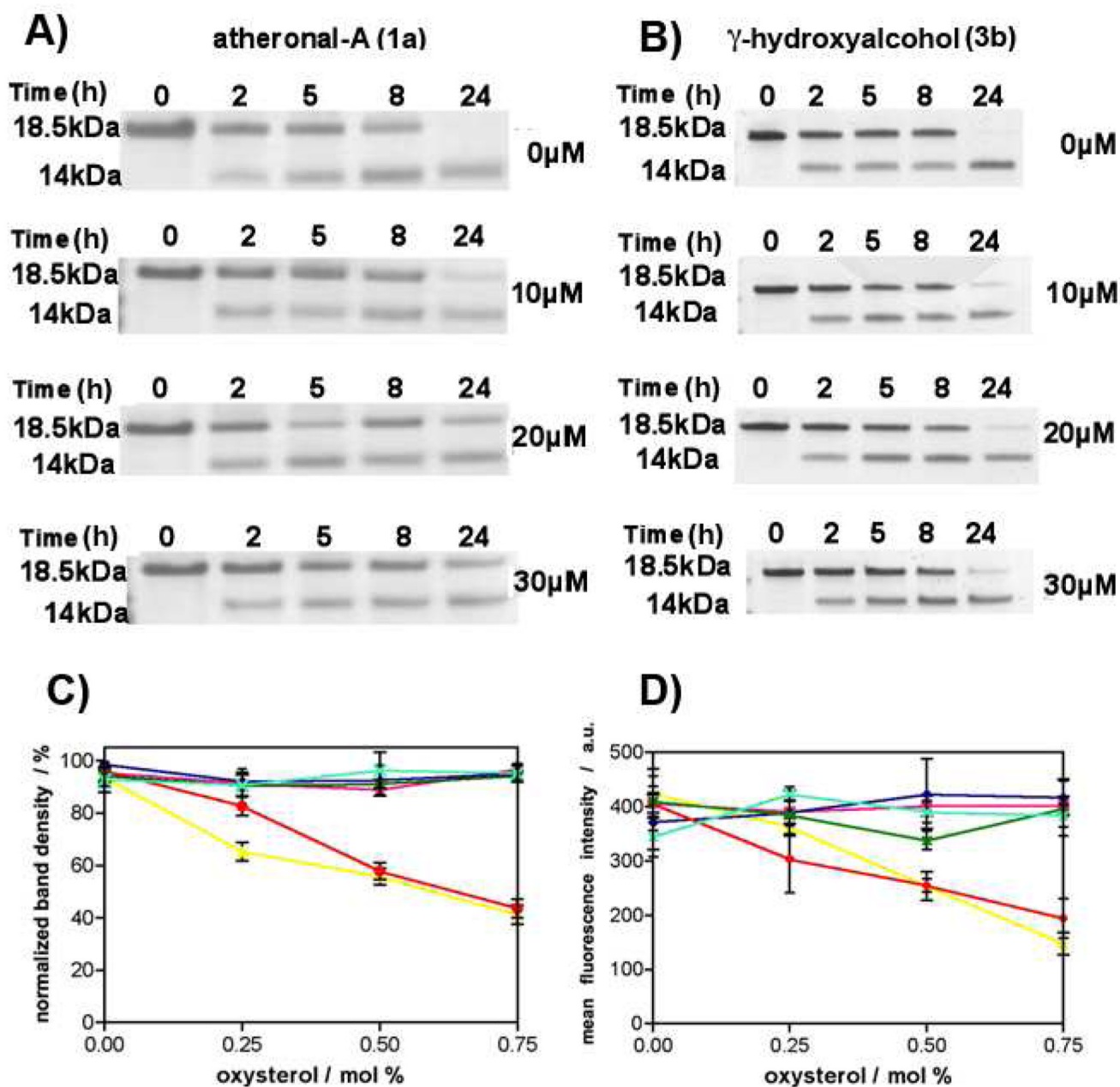
FIGURE 3.

Incorporation of atheronals **1a–b** into cyt-LUVs leads to an increase in surface exposure of the immunodominant epitope (V85-T97) of bMBP. (A) Representative FCM histogram of counts versus log fluorescence intensity for cyt-LUVs bMBP aggregates in the absence (black) or presence of **1a** (0.75 mol %, purple) (B) Graph of MFI \pm S.D versus [**1a–3b**] / mol % measured by flow cytometry (FCM). In a typical experiment bMBP was added to cyt-LUVs (10 mM) that included 0, 0.25, 0.5, and 0.75 mol % of **1a** (













), **2a** (), **2b** (), **3a** (), or **3b** (

) at a protein : lipid ratio of 1 : 600. Fluorescence intensity was measured three times (10,000 counts each run), and the data is reported as mean fluorescence intensity (MFI) \pm S.D. of three collections of three freshly prepared samples.

**FIGURE 4.**

Incorporation of atheronals **1a–b** into cyt-LUVs leads to a decrease in surface exposure of the cathepsin-D binding domain (L36-P50) of bMBP. A) Representative coomassie-stained SDS-PAGE gels showing time-dependent cathepsin-D cleavage of bMBP observed as a loss of the bMBP band at 18.5 kDa and increase of the band at 14 kDa as a function of atheronal-A (**1a**) concentration (0–0.75 mol %) B) Representative coomassie-stained gels showing time-dependent cathepsin-D cleavage of bMBP observed as a loss of the bMBP band at 18.5 kDa and increase of the band at 14 kDa as a function of γ -hydroxyalcohol (**3b**) concentration (0–0.75 mol %) (C) Line graph summarizing the cathepsin-D (100 ng) digestion of bMBP measured as the mean normalized 18.5 kDa band density as a % of t = 0. In a typical




), or **3b** (

) at a protein: lipid ratio of 1:600.. Data is reported as mean \pm SEM of at least triplicate experiments. D) Measurement of MFI of the primary cathepsin D binding site (Leu36-Pro50) of bMBP aggregated in cyt-LUVs that contain varying amounts of **1a–3b** using FCM. bMBP was added to cyt-LUVs (10 mM) incorporated with either 0, 10, 20, or 30 μ M (0, 0.25, 0.5, and 0.75 mol %) of **1a** (







), **1b** (








), **2a** (





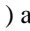


), **2b** (




), **3a** (



), or **3b** (


) at a protein : lipid ratio of 1 : 600. Fluorescence intensity was measured by three collections of 10,000 counts, and the data is reported as the mean fluorescent intensity \pm SEM of three collections of three separate runs.

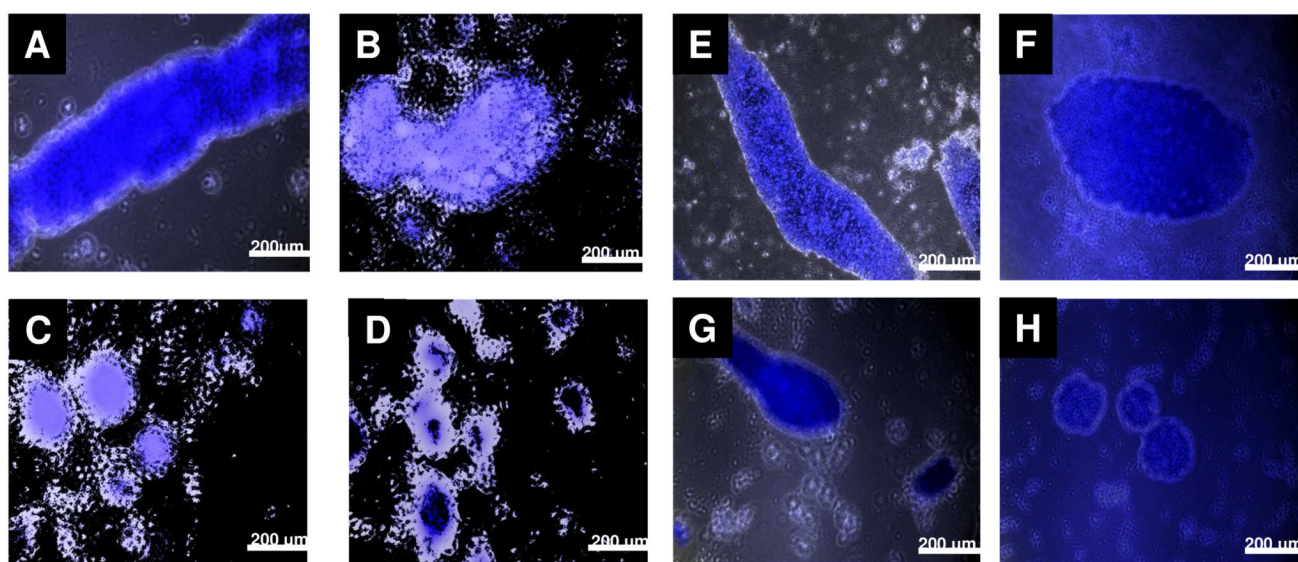


FIGURE 5.

Representative fluorescence microscopy images of bMBP-Cyt-LUV aggregates at a molar protein : lipid ratio of 1 : 600 with varying amounts of **1a** or **1b** incorporated in the LUVs. bMBP was added to cyt-LUVs (HEPES, 20 mM, NaCl, 10 mM; pH 7.4) (50 μ L, 6 mg/mL) containing varying amounts of 1 or 2 (0, 30, 60, or 120 μ M) at a molar protein : lipid ratio of 1 : 600. Please note **1a–b** were added in place of the corresponding mol % of cholesterol. Thioflavin T (ThT) (50 μ M) was added to the LUV suspension which was then allowed to stand for 30 min, added to a viewing slide, dried and imaged. Long fibrous aggregates are observed in control cyt-LUVs (**A, E**). When **1a** (**B–D**) or **1b** (**F–H**) are incorporated into the cyt-LUVs at (30 μ M, 0.75 mol % **B, F**), (60 μ M, 1.50 mol %; **C, G**), or (120 μ M, 3.00 mol %; **D, H**), the aggregates adopt a circular appearance of varying diameter, a clear morphological change relative to control. Three representative images of each sample were taken.

Table 1Effect of atheronals **1a** and **1b** on the size distribution of bMBP-Cyt-LUV aggregates as measured by DLS^a.

	primary size / nm	area / %	secondary size / nm	area / %
control	997.46 ± 27.79	96.23 ± 2.05	45.91 ± 10.41	3.76 ± 2.05
1a	431.49 ± 89.93	73.1 ± 12.33	69.15 ± 42.62	25.08 ± 12.01
1b	463.88 ± 53.69	58.90 ± 3.53	126.42 ± 37.76	41.77 ± 4.79

^abMBP was added to cyt-LUVs (1 mL, 2.5 mM) in the presence or absence of **1a** or **1b** (30 μM, 0.25 mol %) at a 1 : 600 protein : lipid molar ratio and incubated at room temperature for 30 min, and then transferred to a quartz cuvette. Scattered light was detected at a 90° angle to incident irradiation and data was collected from 10 measurements of 5 s duration and averaged utilizing the instrumental software to determine aggregate distribution. The average size for each type of aggregate was measured using data collected from three separate runs. Data are reported as the mean of two major size distributions (nm) with corresponding area (%) ± SD of three collections of three separate runs.